# Polarization of $\Xi^-$ and $\Omega^-$ hyperons produced from neutral beams

D. M. Woods,* P. M. Border, D. P. Ciampa, G. Guglielmo,† K. J. Heller, and N. B. Wallace‡
*School of Physics and Astronomy, University of Minnesota, Minneapolis, Minnesota 55455*

K. A. Johns
*Department of Physics, University of Arizona, Tucson, Arizona 85721*

Y. T. Gao§ and M. J. Longo
*Department of Physics, University of Michigan, Ann Arbor, Michigan 48109*

R. Rameika
*Fermilab, Batavia, Illinois 60510*

(Received 23 February 1996)

We have studied the polarization of $\Xi^-$ and $\Omega^-$ hyperons produced by high energy neutral particle beams. An unpolarized neutral beam striking a target at $\pm 1.8$ mrad produced $1.4 \times 10^7 \Xi^-$'s with an average momentum of 395 GeV/$c$ which were unpolarized, within a sensitivity limit of 0.007, and $2.2 \times 10^5$ $\Omega^-$'s with a polarization of $+0.042 \pm 0.007$ at an average momentum of 374 GeV/$c$. A polarized neutral beam striking a target at 0.0 mrad produced $7.1 \times 10^5 \Xi^-$'s which had a polarization of $-0.118 \pm 0.004$ at an average momentum of 393 GeV/$c$ and $1.8 \times 10^4$ $\Omega^-$'s with a polarization of $-0.069 \pm 0.023$ at an average momentum of 394 GeV/$c$. The polarized neutral beam measurement is in good agreement with a previous measurement. The unpolarized neutral beam results are not understood in the context of the current models of hyperon polarization. [S0556-2821(96)01323-9]

PACS number(s): 13.88.+e, 14.20.Jn

## I. INTRODUCTION

The polarization of hyperons produced from high energy protons was first observed in 1976 for $\Lambda^0$'s [1]. Since then, polarization has also been observed in $\Sigma^+$, $\Sigma^0$, $\Sigma^-$, $\Xi^0$, and $\Xi^-$ hyperons produced by protons [2–6]. Although polarization appears to be a ubiquitous feature of high energy baryon production, there is as yet no explanation based on the fundamental properties of the strong interaction. Several phenomenological models have offered possible explanations of the polarization observed in hyperon production, but the discovery that $\bar{\Xi}^+$ and $\bar{\Sigma}^-$ antihyperons produced by protons are polarized [7,8], while $\bar{\Lambda}$'s and $\Omega^-$'s are not [9,10] appears to contradict even the most qualitative predictions of the existing models [11–13]. Data on the polarization of baryons produced by particles other than protons are scarcer but may give some additional insight into the problem [14].

In this experiment the polarization of $\Xi^-$ and $\Omega^-$ hyperons produced by both polarized and unpolarized neutral particle beams was studied [15]. The neutral beam contained $\Xi^0$'s, $\Lambda^0$'s, neutrons, $K^0$'s, and $\gamma$'s, but the production of high momentum baryons was dominated by the baryons in the beam. In the case of strange particle production by strange baryons, the strange valence quarks needed to produce the final state can come from valence quarks of the incident particle, in contrast with production by protons, where all of the final state strange quarks must be produced in the interaction. This is the first time that the polarization of $\Xi^-$'s and $\Omega^-$'s produced from an unpolarized neutral beam has been measured. This experiment also repeats with higher statistics and at higher momentum a previous measurement of the polarization of the $\Xi^-$'s and $\Omega^-$'s produced from a polarized neutral beam [16]. The use of these data to measure both the magnetic moment of the $\Omega^-$ and $\Xi^-$ has been reported previously [17].

In proton production, the most striking polarization feature can be seen in Fig. 1. In this plot, previous polarization results for production from 400 GeV protons are plotted as a function of momentum. It can be seen that $\Sigma^+$, $\Sigma^0$, and $\Sigma^-$ hyperons produced by high energy protons in the fragmentation region of that proton are positively polarized, while $\Lambda^0$'s, $\Xi^0$'s, and $\Xi^-$'s are negatively polarized [1–6]. Studies of the polarization of $\Omega^-$'s and $\bar{\Lambda}^0$'s produced from protons found no polarization [9,10]. These results are consistent with models in which the polarization of the produced baryon depends on the valence quark structure of both the incident and produced particles.

The polarization of $\Xi^-$ and $\Omega^-$ hyperons produced from a neutral beam containing polarized $\Lambda^0$ and $\Xi^0$ hyperons was found to be similar in both sign and magnitude to the polarization of the neutral beam [10]. This appeared to confirm the importance of the valence quark structure of both the incident and produced particle.

*Present address: Department of Physics, Kansas State University, Manhattan, Kansas 66506.
†Present address: Department of Physics and Astronomy, University of Oklahoma, Norman, Oklahoma 73019.
‡Present address: Instituto Nazionale di Fisica Nucleare, Via Livornese 1291, 56010 San Piero a Grado (PISA), Italy.
§Present address: University of Lanzhou, Lanzhou, China.

 

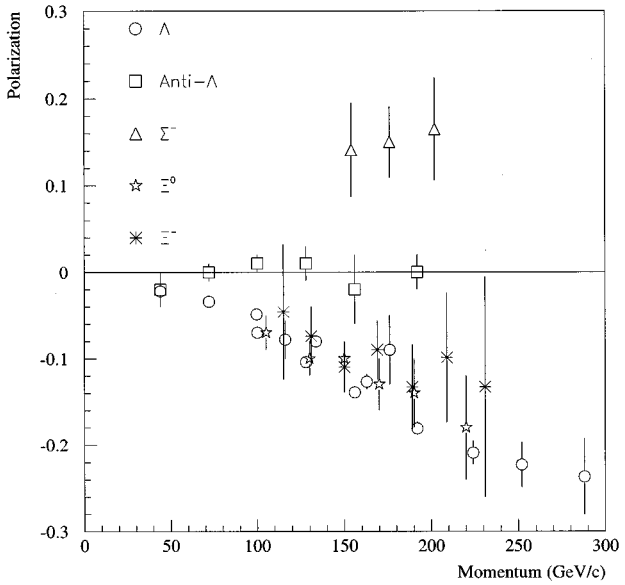


FIG. 1. Hyperon polarization as a function of momentum for production from a 400 GeV proton beam.

Experiments have also studied the polarization of antihyperons, which have no valence quarks in common with the beam particles. $\overline{\Lambda}^0$'s produced by protons were found to be unpolarized [9], while $\overline{\Xi}^+$'s produced by protons had a polarization with the same sign and magnitude as $\Xi^-$'s produced in the same experiment [7]. Studies of proton production of $\overline{\Sigma}^-$'s found a polarization with a similar sign, but of a smaller magnitude than that of comparable $\Sigma^+$ hyperons [8]. To our knowledge no picture of baryon production has been put forth which can accommodate these results.

## II. EXPERIMENTAL METHOD

In this experiment, performed at Fermilab during the 1991–1992 fixed target running period, a beam of 800 GeV/$c$ protons striking a Be target was used to produce a secondary beam. The neutral portion of the secondary beam was magnetically separated, collimated, and used to produce a sample of $\Xi^-$'s and $\Omega^-$'s by striking another Be target. This sample was contained in a negatively charged beam magnetically separated from the other products of the neutral beam interaction and transported through a curved collimator into a spectrometer.

The standard production method used in hyperon polarization experiments is shown in Fig. 2. Here, $\hat{i}$ is the direction of the incident beam, $\hat{j}$ is the direction of the produced particles, and $\theta$ is the production angle. In this experiment, $\hat{j}$ was fixed and $\theta$ was varied by changing the incident beam direction. The only parity-conserving polarization direction is that normal to the production plane defined by $\hat{i}\times\hat{j}$. The sign of the polarization is defined using the conventional right-hand rule. Note that the polarization vector will change sign if the production angle is reversed. This sign reversal is used to experimentally cancel possible apparatus effects in the polarization measurement.

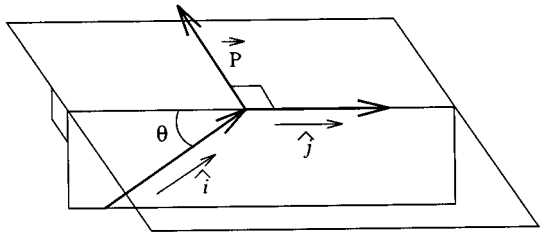


FIG. 2. The standard method of producing polarized hyperons.

### A. Production methods

The 800 GeV proton beam from the Fermilab Tevatron was transported to the proton center targeting area through a series of dipole magnets and quadrupole magnets. The beam arrived at the targeting area as a tightly focused, low divergence beam with a beam spot of approximately 1 $mm^2$. The proton beam position and intensity were monitored using segmented wire ionization chambers (SWIC's) and a secondary emission monitor (SEM).

Figure 3 shows the targeting arrangements for the two production modes used in this experiment. The targeting area consisted of two beryllium targets and two magnets. The two targets were both 150 mm long (0.4 interaction lengths). The upstream target was a cylinder with a diameter of 6.6 mm and the downstream target had a rectangular cross section with a width of 5.2 mm and a height of 5.3 mm. Both targets were mounted on motorized carriers that allowed them to be removed from the beam line during the performance of background studies.

The upstream magnet, M1, contained a collimator that had a straight channel for the selection of a neutral beam with a defining aperture of 2.7 mm $\times$ 2.7 mm $\times$ 914.4 mm. This magnet was mounted on remotely controlled jacks that allowed both ends of the magnet to be raised or lowered to change the production angle at the second target. The second magnet was stationary and contained a collimator with a curved channel that was used to select a negatively charged beam with a central orbit momentum of 394 GeV/$c$ when the magnet was at its full field of 3.3 tesla. The defining aperture

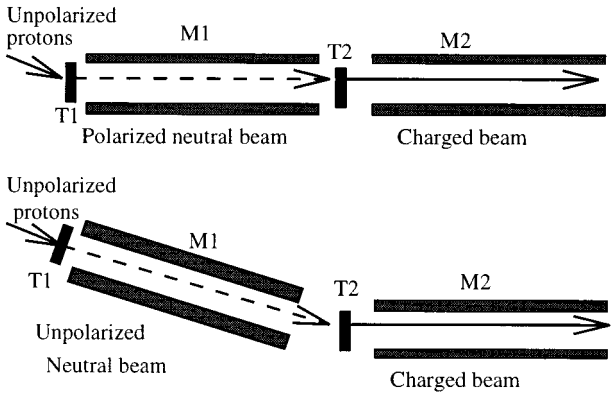


FIG. 3. The two neutral production methods. The top figure shows the polarized neutral beam (PNB) production method and the bottom figure is the unpolarized neutral beam (UNB) production method.

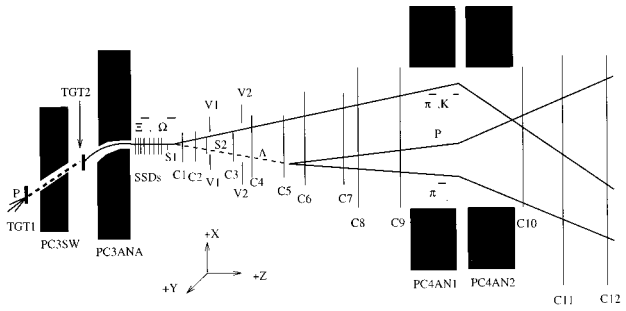


FIG. 4. Plan view of the experiment. The transverse dimensions have been exaggerated. The spectrometer was approximately 80 m long and 3 m wide.

of this magnet was 5.08 mm $\times$ 5.08 mm.

In the polarized neutral beam (PNB) production mode, the upstream magnet had a horizontal field of 1.8 tesla, and the proton beam of $1.0\times10^{12}$ protons per 20 second spill struck the upstream target at a vertical production angle of $\pm1.8$ mrad. The field direction was selected so that the protons were always bent in the direction of the incident beam. The upstream magnet selected a neutral beam containing neutrons, $\Lambda^0$'s, $\Xi^0$'s, $K^0$'s, and $\gamma$'s. In this neutral beam, the $\Lambda^0$'s and $\Xi^0$'s were polarized horizontally due to the nonzero vertical production angle [1,5]. The polarization of the neutrons was unknown. The neutral beam struck the second target at an angle of 0 mrad. The downstream magnet (M2) selected a negatively charged beam. The first magnet did not precess the polarization of the neutral beam since the polarization was along the direction of the magnetic field, while the second magnet precessed the spin of the negatively charged tertiary beam. This spin precession was used to measure the magnetic moments of the $\Xi^-$ and $\Omega^-$ [17].

In the unpolarized neutral beam (UNB) production mode, the upstream magnet (M1) was elevated or lowered to an angle of $\pm1.8$ mrad so that the proton beam of $2.0\times10^{12}$ protons per spill struck the upstream target at an angle of 0 mrad. The upstream magnet selected a neutral beam, which contained unpolarized $\Lambda^0$'s and $\Xi^0$'s. The neutral beam then struck the downstream target at a production angle of $\pm1.8$ mrad and the downstream magnet (M2) selected a negatively charged beam.

### B. The spectrometer

After exiting the second magnet, the charged particles entered the spectrometer, which is shown in Fig. 4 along with the coordinate system. The positions and dimensions of the spectrometer elements are described in Table I. This spectrometer was designed to observe the decays $\Xi^-\rightarrow\Lambda^0\pi^-$ and $\Omega^-\rightarrow\Lambda^0K^-$ with the $\Lambda^0$ decaying to $p\pi^-$. These decay sequences both resulted in a final state with three tracks, one positively charged and two negatively charged.

TABLE I. The size and $z$ positions of the spectrometer elements. All measurements are given in centimeters. Width and height refer to the active area of the detector (n/a = not applicable).

| Detector | Position | Width | Height | Thickness | Pitch | Device type |
|---|---|---|---|---|---|---|
| SSD1(x) | 74.43 | 2.8 | 2.8 | 0.03 | 0.01 | SSD |
| SSD1(y) | 79.22 | 2.8 | 2.8 | 0.03 | 0.01 | SSD |
| SSD2(x) | 100.97 | 2.8 | 2.8 | 0.03 | 0.01 | SSD |
| SSD2(y) | 109.97 | 2.8 | 2.8 | 0.03 | 0.01 | SSD |
| SSD3(x) | 129.46 | 2.8 | 2.8 | 0.03 | 0.01 | SSD |
| SSD3(y) | 137.80 | 2.8 | 2.8 | 0.03 | 0.01 | SSD |
| SSD4(x) | 158.43 | 2.8 | 2.8 | 0.03 | 0.01 | SSD |
| SSD4(y) | 166.29 | 2.8 | 2.8 | 0.03 | 0.01 | SSD |
| S1 | 360.0 | 6.35 | 3.81 | 0.1 | n/a | Scintillator |
| C1(x,y) | 561.0 | 12.8 | 12.8 | n/a | 1.0 | MWPC |
| C2(x,y) | 776.0 | 12.8 | 12.8 | n/a | 1.0 | MWPC |
| V1 | 800.0 | 32.38 | 8.89 | 0.32 | n/a | Scintillator |
| V1(hole) | 800.0 | 11.43 | 6.35 | 0.32 | n/a | n/a |
| S2 | 800.0 | 10.79 | 6.35 | 0.1 | n/a | Scintillator |
| C3(x,y) | 988.0 | 12.8 | 12.8 | n/a | 1.0 | MWPC |
| V2 | 1020.0 | 41.91 | 11.43 | 0.32 | n/a | Scintillator |
| V2(hole) | 1020.0 | 13.97 | 8.25 | 0.32 | n/a | n/a |
| C4(x,y) | 1511.0 | 25.6 | 25.6 | n/a | 1.0 | MWPC |
| C5(x,y) | 2009.0 | 25.6 | 25.6 | n/a | 1.0 | MWPC |
| C6(x,y) | 2499.0 | 51.2 | 25.6 | n/a | 2.0 | MWPC |
| C7(u,v) | 3013.0 | 12.8 | 12.8 | n/a | 2.0 | MWPC |
| C8(u,v) | 3089.0 | 51.2 | 51.2 | n/a | 2.0 | MWPC |
| C9(x,y,u) | 3697.0 | 51.2 | 51.2 | n/a | 2.0 | MWPC |
| C10(x,y) | 4261.0 | 63.8 | 25.6 | n/a | 2.0 | MWPC |
| C11(x,y) | 4840.0 | 128.0 | 38.4 | n/a | 2.0 | MWPC |
| C12(x,y) | 6154.0 | 128.0 | 38.4 | n/a | 2.0 | MWPC |

The spectrometer contained eight planes of silicon strip detectors (SSD's), four scintillators (S1, S2, V1, V2), twelve multiwire proportional chambers (MWPC's), and two analysis magnets (M3, M4). Helium-filled tubes and bags were placed between all elements of the spectrometer to reduce the effect of multiple scattering.

The eight planes of SSD's, four in the $x$ view and four in the $y$ view, were installed as close to the exit of M2 as possible. The first SSD plane was located 0.74 m downstream of the end of M2. The SSD's were arranged in pairs, with each pair containing one $x$ and one $y$ plane separated by 0.048 m, and with a separation of 0.255 m between sets of planes. Each SSD plane had 280 strips with a pitch of 100 $\mu$m. The SSD's were used to track the parent particle and, when the parent decay occurred in the SSD array, its charged daughter particle.

Scintillators S1, V1, S2, and V2 were used as beam trigger and veto counters. S1 and S2 were used to identify particles that had cleanly passed through the collimator in M2. V1 and V2 had holes in their centers and were used to veto particles that were too far from the $z$ axis of the spectrometer and thus had either scattered or were decay products.

Chambers C1–C5 each had horizontal and vertical $(x,y)$ sense planes with 1 mm wire spacing. In chambers C6–C12, the sense plane wire spacing was 2 mm. C6 and C9–C12 each had $x$ and $y$ sense planes. C9 had an additional sense plane that was rotated by 45° with respect to the $z$ axis of the spectrometer. C7 and C8 each had two orthogonal sense planes that were rotated by 45° with respect to the spectrometer $z$ axis. The rotated planes were used in the reconstruction process to match reconstructed $x$ and $y$ tracks. The gas used in the MWPC's was an argon-freon mixture bubbled through methylal at 2° C. The gas mixture was 95% argon, 5% methylal, and 0.12% freon where the percentages are given by gas volume.

Two dipole magnets, M3 and M4, were used to analyze the momentum of all charged particles. The magnets were both 182 cm long and had an $x$ aperture of 61 cm. M3 had a $y$ aperture of 25.4 cm and M4 had a $y$ aperture of 30.5 cm. The magnets were separated by a distance of 56 cm. The field of the two magnets was in the vertical direction providing a momentum kick of 1.445 GeV/$c$ in the $x$-$z$ plane.

The trigger used to detect three-track candidate events consisted of two parts. The first part required hits in S1 and S2 and no hits in V1 or V2. This ensured that a charged particle had entered the spectrometer from the hyperon beam. This part of the trigger was prescaled to record primarily single-track events that were used to align the spectrometer, monitor the efficiency of the various spectrometer elements, and perform other systematic studies. The characteristic ''V'' topology of the $\Lambda^0 \rightarrow p\pi^-$ decay was used to make a loose three-track trigger. This was done by requiring a hit in the negative (right) side of C11 and a hit in the positive (left) side of C12. The three-track trigger was defined as:

$$S1 \cdot S2 \cdot \overline{V1} \cdot \overline{V2} \cdot (C11)_R \cdot (C12)_L . \tag{2.1}$$

When a good three-track trigger occurred, all the hit information from the SSD's and MWPC's was read and recorded. The trigger rate for the experiment was approximately 25 000 triggers per 20 second spill with a livetime of approximately 70%. During approximately six months of running, $1.3\times10^9$ triggers were written to tape.

## III. RECONSTRUCTION AND SELECTION OF EVENTS

The reconstruction process was designed to find events with a good three-track, two-vertex topology. Since the trigger requirements were made as loose as possible to avoid biasing the data sample, only a small portion of the events recorded were of interest. For events where a three-track, two-vertex topology could be found, kinematic variables, including the parent and daughter $\Lambda^0$ vertices and the momentum of all the particles, were determined. The mass of the parent particle was calculated under both the $\Xi^-$ and $\Omega^-$ hypotheses.

The polarization measurement was made by studying the asymmetries in the angular distributions of the daughter protons in the $\Lambda$ rest frame. For this reason, it was important that the data selection process includes as few misreconstructed events as possible since these events could affect the measured asymmetries. Monte Carlo studies were made to identify data selection criteria that could be used to remove events that the reconstruction process was likely to misreconstruct. A primary and two secondary reconstruction strategies were used with the secondary strategies applied to those events that were likely to be misreconstructed by the primary or the other secondary strategy.

In all of the reconstruction strategies, the MWPC hit information was used to reconstruct the daughter particle tracks. Then, when the parent decay did not occur in the region near the SSD's, the SSD hit information was used to reconstruct the track of the parent or its charged daughter. The momentum of the three daughters was calculated from the bend of the tracks as they passed through the analysis magnets. These momenta were used to calculate the momentum of both the parent particle and the daughter $\Lambda^0$. From these momenta, the mass of the parent, the mass of the $\Lambda^0$, the position of the parent at the production target, and the parent and $\Lambda^0$ decay vertices were calculated. The information from the $\Lambda^0$ decay products was a fit to a single-vertex event topology that was forced to have the known $\Lambda^0$ mass.

The first reconstruction strategy used the MWPC hits to make tracks starting at the most downstream chambers where the particles were well separated. This strategy assigned hits to tracks based on the expected topology and was very fast. It correctly reconstructed approximately 67% of the final data sample. The second strategy consisted of finding multiple solutions for the three-daughter, two-vertex topology and choosing the one that gave the best mass fit for the parent and $\Lambda^0$. This strategy was used for 20% of the final data sample. The remaining 13% of the final data sample was reconstructed using a third strategy. This method started with the SSD and upstream chamber information to find the parent vertex and eliminate the charged daughter meson from the topology, thus leaving a less-complicated, two-track, one-vertex topology to fit. Monte Carlo studies showed that together, these three strategies correctly reconstructed over 98% of the events which were included in the final data sample.

Good events were selected from the reconstructed three-

track events using several selection criteria. The reconstructed event was required to have a mass that was within 15 MeV/$c^2$ of either the known $\Xi^-$ or the known $\Omega^-$ mass. The $\Xi^-$ or $\Omega^-$ was required to originate less than 0.9 cm in $x$ and 0.8 cm in $y$ from the center of the production target. The event was also required to be a good fit to the three-track topology ($\chi^2$/degree of freedom $<4$) and a good kinematic fit to the $\Lambda$. In addition, no hit from the MWPC's was allowed to be used on more than one track, and at least two hits were required in the $x$ planes of C6, C9–C11 and in the $y$ planes of C6, C9, and C10.

The main physics background for the $\Xi^-$ events was $K^-\to 3\pi$ decays. However, Monte Carlo studies showed that these events would be reduced to less than 0.01% by the trigger and reconstruction process. An additional possible source of background for the $\Xi^-$ sample was the decay $\Omega^-\to\Lambda^0 K^-$. However, since $\Xi^-$'s were produced approximately 100 times more often than $\Omega^-$'s, and most $\Omega^-$'s did not reconstruct with the known $\Xi^-$ mass, this background was less than 0.3%.

The backgrounds for the $\Omega^-$ sample were a more serious problem. In addition to the $\Xi^-\to\Lambda^0\pi^-$ and $K^-\to 3\pi$ decays, other possible sources of background were $\Omega^-\to\Xi^0\pi^-$ with $\Xi^0\to\Lambda^0\pi^0$ and $\Omega^-\to\Xi^-\pi^0$ decays. Monte Carlo studies showed that the reconstructed $\Omega^-$ sample contained approximately 10.5 $\Xi^-\to\Lambda^0\pi^-$ decays and 0.017 $\Omega^-\to\Xi^0\pi^-$ decays for each $\Omega^-\to\Lambda^0 K^-$ decay. The background due to $\Omega^-\to\Xi^-\pi^0$ and $K^-\to 3\pi$ decays was found to be insignificant. The background in the $\Omega^-$ sample could be greatly reduced by selecting data based on the opening angles, $\cos\theta_K=\hat{K}^-\cdot\hat{z}$ and $\phi_K=\arctan(\hat{K}^-\cdot\hat{y}/\hat{K}^-\cdot\hat{x})$, of the kaon in the rest frame of the $\Omega^-$. When events with $\cos\theta_K>0.775$ and $\cos\theta_K<(|0.008125\times\phi_K|-1.8125)$ were removed, Monte Carlo simulation estimated the background to be 0.25% due to $\Xi^-$ decays and 1.61% due to $\Omega^-\to\Xi^0\pi^-$ decays. The actual background, estimated from the tails of the mass plots, was approximately 3% [17–19].

## IV. POLARIZATION ANALYSIS

In the decays $\Xi^-\to\Lambda^0\pi^-$ and $\Omega^-\to\Lambda^0 K^-$, the polarization of the parent particle, $\vec{P}_\Xi$ or $\vec{P}_\Omega$, can be related to the polarization of the daughter $\Lambda^0$, $\vec{P}_\Lambda$. This, in turn, is extracted from the distribution of the protons from the $\Lambda^0$ decay.

The weak decay $\Xi^-\to\Lambda^0\pi^-$ has a spin $\frac{1}{2}$ parent going to spin $\frac{1}{2}$ and spin 0 daughter particles. The $\Xi^-$ polarization $\vec{P}_\Xi$ is related to the daughter $\Lambda$ polarization $\vec{P}_\Lambda$ by [20]

$$\vec{P}_\Lambda=\frac{(\alpha_\Xi+\hat{\Lambda}\cdot\vec{P}_\Xi)\hat{\Lambda}+\beta_\Xi(\vec{P}_\Xi\times\hat{\Lambda})+\gamma_\Xi(\hat{\Lambda}\times\vec{P}_\Xi)\times\hat{\Lambda}}{1+\alpha_\Xi\hat{\Lambda}\cdot\vec{P}_\Xi}. \tag{4.1}$$

Here, $\hat{\Lambda}$ is the direction of the $\Lambda^0$ in the $\Xi^-$ rest frame and $\alpha_\Xi$, $\beta_\Xi$, and $\gamma_\Xi$ are the weak decay parameters for the decay $\Xi^-\to\Lambda^0\pi^-$.

Time-reversal invariance arguments require $\beta_\Xi=0$ [21], and due to the symmetry of the spectrometer about the beam axis, the average value of $\hat{\Lambda}$ projected onto any spatial axis will be small. The terms involving $\hat{\Lambda}\cdot\vec{P}_\Xi$ were considered in a second iteration and found to have no effect on the measured polarization values. These arguments simplify Eq. (4.1) to

$$\vec{P}_\Lambda=\alpha_\Xi\hat{\Lambda}+\gamma_\Xi\vec{P}_\Xi. \tag{4.2}$$

For the $\Lambda$ decay, the normalized distribution of the daughter proton in the parent ($\Lambda$) rest frame is

$$\frac{dn_p}{d\Omega}=\frac{1}{4\pi}(1+\alpha\vec{P}\cdot\hat{p}), \tag{4.3}$$

where $\vec{P}$ is the polarization of the parent $\Lambda$, $\hat{p}$ is the direction of the daughter proton in the rest frame of the parent, and $\alpha$ is the appropriate weak decay asymmetry parameter [19]. If Eq. (4.3) is expressed in spherical coordinates and integrated over $\phi$,

$$\frac{dn_p}{d(\cos\theta_i)}=\frac{1}{2}(1+\alpha_\Lambda P_{\Lambda i}\cos\theta_i), \tag{4.4}$$

where $P_{\Lambda i}$ is the polarization along an axis $\hat{i}$ and $\theta_i$ is the angle between $\hat{p}$ and $\hat{i}$. This expression can be combined with Eq. (4.2) to find the relation between the proton distribution and the polarization of the parent $\Xi^-$:

$$\frac{dn_p}{d(\cos\theta_i)}=\frac{1}{2}[1+(\alpha_\Lambda\alpha_\Xi\Lambda_i+\alpha_\Lambda\gamma_\Xi P_{\Xi i})\cos\theta_i]. \tag{4.5}$$

The $\Omega^-$ is assumed to be a spin $\frac{3}{2}$ particle, but a similar relation between $\vec{P}_\Omega$ and $\vec{P}_\Lambda$ can be derived [22]:

$$\vec{P}_\Lambda=\frac{1+4\gamma_\Omega}{5}\vec{P}_\Omega. \tag{4.6}$$

Since $\alpha_\Omega$ is small [23] and time-reversal invariance requires $\beta_\Omega=0$, $|\gamma_\Omega|\approx 1$. A value of $\gamma_\Omega=+1$ is predicted by theory [24] and also favored by the experimental data [19], leading to the result $P_\Lambda=P_\Omega$. Substituting the above expression into Eq. (4.4) gives the relationship between the proton distribution and $P_\Omega$:

$$\frac{dn_p}{d(\cos\theta_i)}=\frac{1}{2}(1+\alpha_\Lambda P_\Omega\cos\theta_i). \tag{4.7}$$

With these expressions relating the proton angular distributions $\cos\theta_i$ to the polarization of the parent, the observed distributions of the $\Xi^-$ and $\Omega^-$ decay products could be fit and the polarizations extracted. The decay distributions were corrected for the finite acceptances of both the spectrometer and the reconstruction process using a hybrid Monte Carlo technique [25]. This technique maps the experimental acceptance in $\cos\theta_i$ by generating a number of fake events for each real event. The fake events are identical to the real events except that their $\cos\theta_i$ values are chosen randomly, thereby changing the daughter proton and $\pi^-$ momenta in the laboratory. The fake events are then subjected to all of the spectrometer apertures, trigger requirements, and data selection

TABLE II. Measured $\Xi^-$ asymmetries as a function of momentum for data with 0 mrad production angle at both targets. The errors given in the table are the statistical errors only.

| Momentum (GeV/$c$) | Asymmetry $\alpha_\Lambda \gamma_\Xi P_{\Xi x}$ | $\alpha_\Lambda \gamma_\Xi P_{\Xi y}$ | $\alpha_\Lambda \gamma_\Xi P_{\Xi z}$ |
|---|---|---|---|
| 347 | $-0.0018 \pm 0.0053$ | $0.0103 \pm 0.0056$ | $0.0072 \pm 0.0067$ |
| 367 | $-0.0102 \pm 0.0042$ | $0.0014 \pm 0.0047$ | $0.0041 \pm 0.0052$ |
| 383 | $0.0006 \pm 0.0038$ | $0.0020 \pm 0.0042$ | $0.0089 \pm 0.0048$ |
| 399 | $-0.0021 \pm 0.0038$ | $-0.0012 \pm 0.0042$ | $0.0049 \pm 0.0048$ |
| 418 | $-0.0010 \pm 0.0036$ | $0.0030 \pm 0.0038$ | $0.0037 \pm 0.0044$ |
| 455 | $-0.0005 \pm 0.0038$ | $0.0014 \pm 0.0039$ | $0.0070 \pm 0.0047$ |

criteria that the real event was required to pass. The polarization of the fake events is then varied to find the best fit to the data.

The value of the asymmetry measured with this method is the sum of two contributions. These are the real polarization signal and a ''bias'' term due to acceptances of the spectrometer and reconstruction process that could not be simulated in the hybrid Monte Carlo. These biases do not depend on the sign of the production angles. However, the polarization does change sign when the production angle is reversed. The measured asymmetries for the positive and negative production angle, $A_+$ and $A_-$, can be expressed in terms of the bias $B$ and polarization components $\alpha_\Lambda \gamma_\Xi P_\Xi$ as

$$A_\pm = B \pm \alpha_\Lambda \gamma_\Xi P_\Xi . \tag{4.8}$$

The bias and real signal components can then be extracted:

$$\alpha_\Lambda \gamma_\Xi P_\Xi = \frac{A_+ - A_-}{2}, \tag{4.9}$$

$$B = \frac{A_+ + A_-}{2}. \tag{4.10}$$

Similar expressions were used in the $\Omega^-$ analysis. Typical biases were less than 3% for both the $\Xi^-$ and $\Omega^-$ samples.

The production polarization was determined from the measured $x$ and $z$ components, $P_x$ and $P_z$, by finding the value of $P_{\rm tgt}$ that minimized the function:

$$\chi^2 = \frac{(P_x - P_{\rm tgt}\cos\Phi)^2}{\sigma_x^2} + \frac{(P_z - P_{\rm tgt}\sin\Phi)^2}{\sigma_z^2}, \tag{4.11}$$

where $\sigma_x$ and $\sigma_z$ are the statistical errors for the $x$ and $z$ components of the polarization, and $\Phi$ is the precession angle in magnet M2:

$$\Phi = \frac{e}{\beta m_h c}\left(\frac{m_h}{m_p}\frac{\mu_h}{2J\mu_N} + 1\right)\int Bdl. \tag{4.12}$$

Here, $e$ is the magnitude of the electron charge, $\beta = v/c$, $m_p$ is the mass of the proton, $m_h$ is the mass of the hyperon, $\mu_h$ is the magnetic moment of the hyperon in nuclear magnetons ($\mu_N$), $J$ is the spin of the hyperon, and $\int Bdl$ is the field integral of the precession magnet (M2) in tesla-meters (T-m). When the precession magnet current was set at $-750$ amps, the $\int Bdl$ is $-17.48$ T-m. For data taken with the current in the precession magnet at $-2900$ amps, the $\int Bdl$ was $-24.36$ T-m.

## V. RESULTS AND CONCLUSIONS

All of the $\Xi^-$ and $\Omega^-$ candidate events from both the polarized and unpolarized neutral beam production modes were analyzed. The unpolarized neutral beam sample consisted of $1.4 \times 10^7 \Xi^-$ and $2.2 \times 10^5 \Omega^-$ events. The polarized neutral beam sample contained $7.1 \times 10^5 \Xi^-$'s and $1.8 \times 10^4 \Omega^-$'s.

### A. Systematic studies

To search for possible systematic effects, several different studies were undertaken. Studies were also performed to test the sensitivity of our measurement and determine the experiment's ability to measure nonzero polarization results.

Events produced from a neutral beam with a 0 mrad production angle at both targets were analyzed. These events should be unpolarized and were used to determine the sensitivity of our polarization analysis technique and to search for residual polarization. Potential sources of residual polarization included limitations on how accurately the production angle could be controlled and production from the sides of the neutral collimator. The $\Xi^-$ asymmetry results for this production mode are given in Table II. The production polarization is $0.007 \pm 0.003$.

A study of the targeting arrangement showed that a small deviation from a 0 mrad production angle at the first target or production off the neutral collimator could produce a neutral beam with a small residual polarization. This polarization could then be transferred to charged events produced at the second target. This small residual polarization would limit the ability of the experiment to measure the polarization of samples with very small or zero polarization. Therefore, a

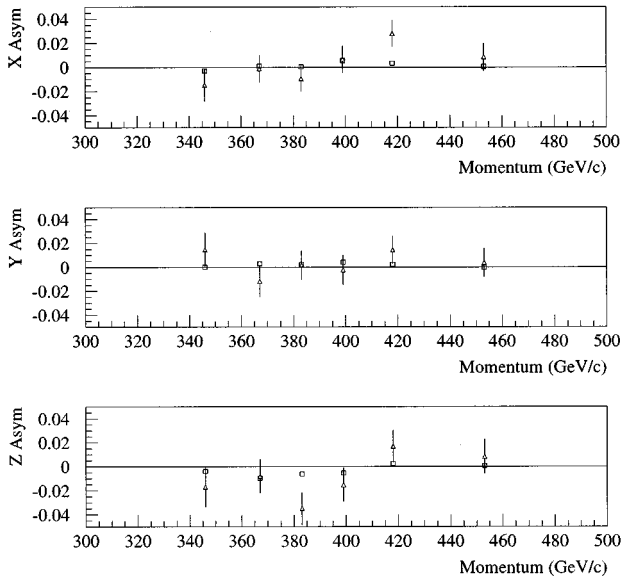


FIG. 5. Comparison of asymmetry ($\alpha_\Lambda \gamma_\Xi P_\Xi$) components for the single-track (triangles) and three-track (squares) triggers from the unpolarized neutral beam data sample.

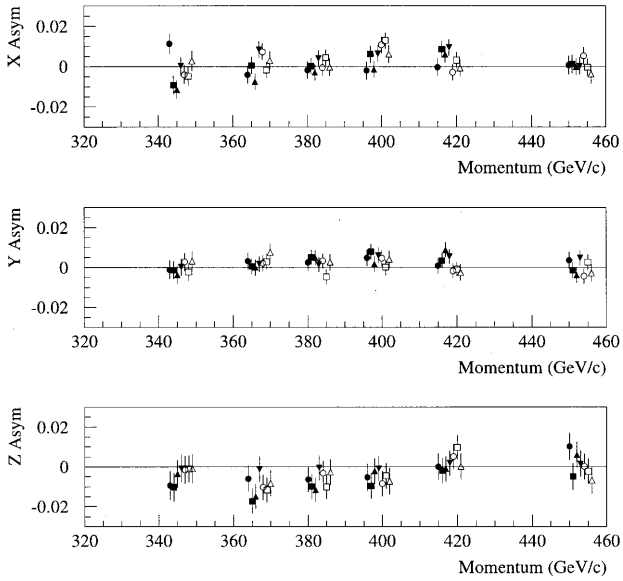


FIG. 6. Comparison of asymmetry ($\alpha_\Lambda \gamma_\Xi P_\Xi$) components for the seven subsamples of the unpolarized neutral beam data sample.

limit of 0.007 is placed on our ability to measure zero polarization.

Based on an analysis of possible sources of residual polarization, it was found that the largest effect would occur in the unpolarized neutral beam production mode. Here the residual neutral beam polarization would be similar to the polarized neutral beam in the PNB production mode. In the polarized neutral beam production mode, any residual neutral beam polarization would be indistinguishable from polarization due to the nonzero production angle at the first target. For the $\Omega^-$ sample, the effect of the residual asymmetry is reduced because of the different asymmetry parameters. In addition, the results for the polarized neutral beam production mode show that for a given neutral beam polarization, the $\Omega^-$'s have a smaller polarization than that for the $\Xi^-$'s.

The effect of a residual polarization on the $\Omega^-$ magnetic moment measurement was also studied. The magnetic moment measurement assumes that the polarization is produced along the $x$ axis, as required by parity conservation, and then precesses into the $x$-$z$ plane as the beam passes through the magnetic field. Therefore, only a residual polarization along the $z$ axis will have an adverse effect on the magnetic moment measurement. The residual polarization produced along the $z$ axis was estimated from the $z$ asymmetry of the 0 mrad data sample. This residual polarization was found to be a factor of 5 smaller than the error in the $z$ component of the measured $\Omega^-$ polarization, and thus was deemed negligible in this experiment.

To search for possible systematic effects due to the trigger requirements, single-track triggers from the UNB sample which relied only on the scintillation counters were subjected to the polarization analysis. Figure 5 shows the measured asymmetry components for $\Xi^-$'s collected using the single-track trigger compared to the $\Xi^-$ asymmetry components for three-track trigger events in the same data sample. There is no evidence for any trigger-induced effect in the data. Another possible source of systematic effects was undetected changes in experimental conditions over the course of the data collection period which spanned several months. These might include changes in the efficiencies of the MWPC's and SSD's, variations in the fields of the four magnets used in the experiment, or variations in the efficiencies of the trigger counters. To search for these effects, the sample of $\Xi^-$'s produced using the unpolarized neutral beam was divided chronologically into seven subsamples. Figure 6 shows the asymmetry components of the seven unpolarized neutral beam production subsamples plotted as a function of momentum. No evidence of a time-dependent systematic effect was found.

To ensure that the data selection criteria used had not added systematic asymmetries to the results, the effect of tightening the various data selection criteria was studied. This was done using the $\Xi^-$ sample produced from the polarized neutral beam. Each of the selection criteria was varied, and the effect of the variation on the measured value of the $\Xi^-$ magnetic moment was studied. No evidence of any systematic effect due to the data selection criteria was found.

### B. Unpolarized neutral beam production

For production using an unpolarized neutral beam, data were taken at two different current settings in the precession magnet (M2). This allowed a larger momentum range to be explored and also provided a second $\int Bdl$ point for the magnetic moment measurement. Table III contains the measured $x$ and $z$ asymmetries for the $\Xi^-$ and the production polarization values. For the data with a precession magnet current of $-750$ amps, the production polarization is $-0.010 \pm 0.002$. For the data with a current of $-2900$ amps in the precession magnet, the production polarization is $0.006 \pm 0.002$. This data shows that the $\Xi^-$'s appear to be unpolarized at the level of our sensitivity of 0.007. The $\Omega^-$ pro-

TABLE III. The $x$ and $z$ components of the $\Xi^-$ asymmetry and the production polarization as a function of momentum for the unpolarized neutral beam production mode. The errors given in the table are the statistical errors only.

| Precession magnet (M2) current | Momentum (GeV/$c$) | Number of events | $\alpha_\Lambda \gamma_{\Xi^-} P_x$ | $\alpha_\Lambda \gamma_{\Xi^-} P_z$ | Production polarization |
|---|---|---|---|---|---|
| −750 | 260 | 730548 | −0.006 ± 0.002 | −0.004 ± 0.003 | −0.010 ± 0.004 |
| −750 | 282 | 812813 | −0.003 ± 0.002 | −0.006 ± 0.003 | −0.003 ± 0.003 |
| −750 | 299 | 826500 | −0.007 ± 0.002 | −0.006 ± 0.002 | −0.010 ± 0.003 |
| −750 | 318 | 744609 | −0.005 ± 0.002 | 0.000 ± 0.003 | −0.009 ± 0.004 |
| −750 | 349 | 645241 | −0.008 ± 0.002 | 0.007 ± 0.003 | −0.017 ± 0.004 |
| −2900 | 346 | 1392868 | −0.003 ± 0.002 | −0.004 ± 0.002 | −0.003 ± 0.003 |
| −2900 | 367 | 1654941 | 0.001 ± 0.001 | −0.010 ± 0.002 | 0.007 ± 0.002 |
| −2900 | 383 | 1792954 | 0.001 ± 0.001 | −0.006 ± 0.002 | 0.004 ± 0.002 |
| −2900 | 399 | 1683542 | 0.006 ± 0.001 | −0.005 ± 0.002 | 0.012 ± 0.002 |
| −2900 | 418 | 1813517 | 0.003 ± 0.001 | 0.002 ± 0.002 | 0.004 ± 0.002 |
| −2900 | 454 | 1633080 | 0.001 ± 0.001 | 0.001 ± 0.002 | 0.001 ± 0.003 |

duction polarization data as a function of momentum for this production method are given in Table IV. This table clearly shows that the $\Omega^-$'s are polarized. Figure 7 shows the measured precession angles of the $\Xi^-$'s and $\Omega^-$'s $[\Phi = \arctan(P_z/P_x)]$ along with the expected precession angle calculated using the known $\int Bdl$ and magnetic moment. For comparison, the precession angles for the $\Xi^-$ sample produced with 0 mrad production angles at both targets are also shown. This figure shows that the measured $\Xi^-$ precession angles for this sample and for the sample produced with 0 mrad production angles at both targets vary considerably from the value calculated from the $\Xi^-$ magnetic moment as would be expected if the samples were unpolarized. However, the $\Omega^-$ precession angles agree with the expected value, as expected for a polarized sample. For the entire $\Omega^-$ sample , the production polarization is $+0.042 \pm 0.007$ at an average momentum of 374 GeV/$c$.

### C. Polarized neutral beam production

The polarization results for the polarized neutral beam production mode are given in Tables V and VI. Both samples were found to be polarized, as expected from a previous measurement [16]. The measured production polarizations for the entire sample were $-0.118 \pm 0.004$ at an average momentum of 393 GeV/$c$ for the $\Xi^-$'s, and $-0.069 \pm 0.023$ at an average momentum of 393 GeV/$c$ for the $\Omega^-$.

Figure 8 shows all of the polarization results of this experiment plotted as a function of momentum.

### D. Conclusions

We have made the first observation of the polarization of $\Xi^-$ and $\Omega^-$ hyperons produced from an unpolarized neutral beam containing strange hyperons. We found that $\Xi^-$'s are unpolarized, at the level of our sensitivity of 0.007, and that $\Omega^-$'s have a polarization of $+0.042 \pm 0.007$ at an average momentum of 374 GeV/$c$. We have also repeated, with greater precision, and at higher momenta, a previous study of the polarization of hyperons produced from a polarized neutral hyperon beam [16], and find a good agreement between the two measurements. Using this production method, $\Xi^-$'s were found to have a polarization of -0.118 ± 0.004 at an average momentum of 393 GeV/$c$ and $\Omega^-$'s had a polar-

TABLE IV. $\Omega^-$ production polarization as a function of momentum for the unpolarized neutral beam production mode. The errors given in the table are the statistical errors only.

| Precession magnet (M2) current | Momentum (GeV/$c$) | Number of events | Production polarization |
|---|---|---|---|
| −750 | 260 | 10004 | +0.030 ± 0.036 |
| −750 | 288 | 14956 | +0.072 ± 0.025 |
| −750 | 312 | 12604 | +0.047 ± 0.026 |
| −750 | 349 | 12632 | −0.012 ± 0.028 |
| −2900 | 348 | 42569 | +0.052 ± 0.016 |
| −2900 | 380 | 42487 | +0.027 ± 0.014 |
| −2900 | 403 | 37215 | +0.057 ± 0.015 |
| −2900 | 443 | 44256 | +0.048 ± 0.015 |

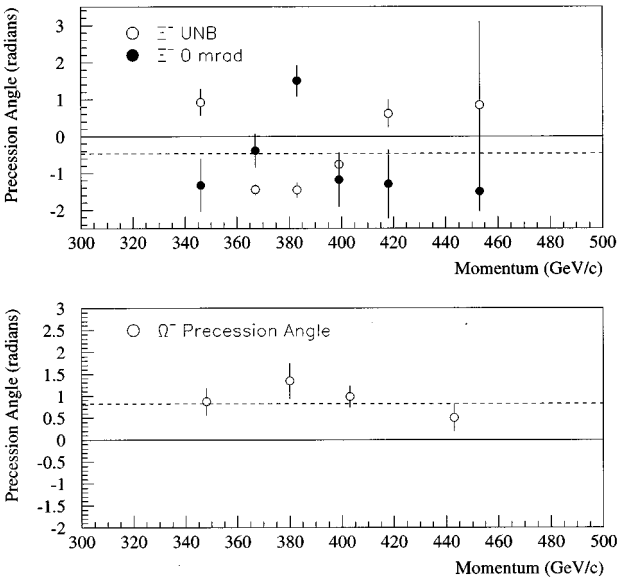


FIG. 7. The measured precession angles in radians for $\Xi^-$'s and $\Omega^-$'s produced from an unpolarized neutral beam (UNB) with a current of $-2900$ amps in the charged sweeper magnet. The precession angles for $\Xi^-$'s produced with a 0 mrad production angle at both targets are also shown. The indicated errors are statistical only. The dashed lines show the expected precession angles calculated using the known magnetic moments.

ization of $-0.069 \pm 0.023$ at an average momentum of 394 GeV/$c$. It is interesting to note that from the polarized neutral beam results presented in Tables V and VI one can see that the $\Xi^-$ polarization is larger at higher momenta while the $\Omega^-$ polarization appears to be constant.

Both of the new measurements resulting from this experiment are surprising. The unpolarized $\Xi^-$'s produced at an angle of 1.8 mrad from an unpolarized neutral beam represent the first time that high energy baryons containing some of the valence quarks of the baryons of which they are fragments, are not polarized. One possible explanation is that the $\Xi^-$'s are primarily produced by $\Xi^0$'s, a process that does not involve the production of strange quarks. The implication is that the light $u$ and $d$ quarks are not produced in a polarized state. It is interesting to note that results from another experiment using an unpolarized $\Sigma^-$ beam to produce

TABLE V. $\Xi^-$ production polarization as a function of momentum for the polarized neutral beam production mode. The errors given in the table are the statistical errors only.

| Momentum (GeV/$c$) | Number of events | Production polarization |
|---|---|---|
| 347 | 92534 | $-0.076 \pm 0.011$ |
| 367 | 125268 | $-0.103 \pm 0.009$ |
| 383 | 138491 | $-0.130 \pm 0.008$ |
| 399 | 128636 | $-0.107 \pm 0.009$ |
| 417 | 129950 | $-0.136 \pm 0.009$ |
| 451 | 96467 | $-0.166 \pm 0.011$ |

TABLE VI. $\Omega^-$ production polarization as a function of momentum for the polarized neutral beam production mode. The errors given in the table are the statistical errors only.

| Momentum (GeV/$c$) | Number of events | Production polarization |
|---|---|---|
| 351 | 4535 | $-0.102 \pm 0.049$ |
| 380 | 5060 | $-0.001 \pm 0.042$ |
| 404 | 4298 | $-0.100 \pm 0.045$ |
| 440 | 4428 | $-0.087 \pm 0.046$ |

$\Lambda^0$'s, $\overline{\Lambda^0}$'s, $\Sigma^+$'s, and $\overline{\Xi}^-$'s indicated that the $\Xi^-$'s had a polarization comparable to that of $\Lambda^0$'s produced from a proton beam, but the $\Lambda^0$'s and $\Sigma^+$'s, for which the strange quarks came only from the beam, had noticeably smaller polarizations [26].

The positive polarization found for the $\Omega^-$ is the first time that a produced $s$ quark incorporated into a baryon fragment did not have negative polarization (although $\Sigma$'s produced by protons are positively polarized, the valence $s$ quark in their wave function has a negative polarization). This $\Omega^-$ result seems to rule out the generalization that all strange quarks produced in a strong interaction and incorporated into a baryon have a negative polarization.

It is unfortunate that information on the composition, polarization, and momentum distribution of the neutral beam was not available. However, the results of this experiment, when added to the growing body of high energy strong interaction polarization data, clearly indicate that we are a long way from understanding the polarization mechanisms of the strong interaction.

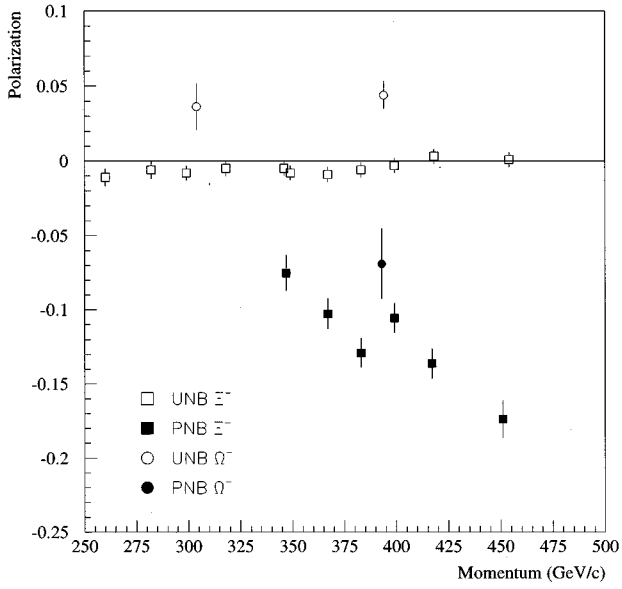


FIG. 8. The measured polarizations as a function of momentum for both the polarized (PNB) and unpolarized (UNB) neutral beam samples of $\Xi^-$'s and $\Omega^-$'s. The indicated errors are statistical only.

**ACKNOWLEDGMENTS**

This work was supported by the U.S. Department of Energy and the National Science Foundation. We would like to thank G. Allan, A. Ayala-Mercado, E. Berman, V. DeCarlo, D. Fein, M. Groblewski Higgins, J. Jallian-Marian, E. James, R. McGriff, L. Morris, T. Tynan, and the staff of Fermi National Laboratory for their assistance.

[1] G. Bunce *et al.*, Phys. Rev. Lett. **36**, 1113 (1976).
[2] C. Ankenbrandt *et al.*, Phys. Rev. Lett. **51**, 863 (1983); C. Wilkinson *et al.*, *ibid.* **58**, 855 (1987); A. Morelos *et al.*, *ibid.* **71**, 2172 (1993).
[3] E. C. Dukes *et al.*, Phys. Lett. B **193**, 135 (1987); B. E. Bonner *et al.*, *ibid.* **62**, 1591 (1989).
[4] L. Deck *et al.*, Phys. Rev. D **28**, 1 (1983); Y. W. Wah *et al.*, Phys. Rev. Lett. **55**, 2551 (1985).
[5] K. Heller *et al.*, Phys. Rev. Lett. **51**, 2025 (1983).
[6] R. Rameika *et al.*, Phys. Rev. D **33**, 3172 (1986); L. H. Trost *et al.*, *ibid.* **40**, 1703 (1989); J. Duryea *et al.*, Phys. Rev. Lett. **67**, 1193 (1991).
[7] P. M. Ho *et al.*, Phys. Rev. Lett. **65**, 1713 (1990).
[8] A. Morelos *et al.*, [2].
[9] K. Heller *et al.*, Phys. Rev. Lett. **41**, 607 (1978).
[10] K. B. Luk *et al.*, Phys. Rev. Lett. **70**, 900 (1993).
[11] T. A. DeGrand and H. I. Miettinen, Phys. Rev. D **23**, 1227 (1981).
[12] B. Andersson *et al.*, Phys. Lett. B **85B**, 417 (1979).
[13] J. Szwed, Phys. Lett. **105B**, 403 (1981); W. G. D. Dharmaratna and G. R. Goldstein, Phys. Rev. D **41**, 1731 (1990); J. Soffer and N. A. Törnqvist, Phys. Rev. Lett. **68**, 907 (1992); R. Barni, G. Preparata, and P. G. Ratcliffe, Phys. Lett. B **296**, 251 (1992).
[14] S. U. Chung *et al.*, Phys. Rev. D **11**, 1010 (1975); J. Bensinger *et al.*, Phys. Rev. Lett. **50**, 313 (1983); S. A. Gourlay *et al.*, *ibid.* **56**, 2244 (1986).
[15] D. M. Woods, Ph.D. thesis, University of Minnesota, 1995.
[16] H. T. Diehl *et al.*, Phys. Rev. Lett. **67**, 804 (1991).
[17] N. B. Wallace *et al.*, Phys. Rev. Lett. **74**, 3732 (1995).
[18] N. B. Wallace, Ph.D. thesis, University of Minnesota, 1995.
[19] G. M. Guglielmo *et al.*, (unpublished); G. M. Guglielmo, Ph.D. thesis, University of Minnesota, 1994.
[20] T. D. Lee and C. N. Yang, Phys. Rev. **108**, 1645 (1957).
[21] O. E. Overseth and S. Pakvasa, Phys. Rev. **184**, 1663 (1969).
[22] K. B. Luk *et al.*, Phys. Rev. D **38**, 19 (1988).
[23] Particle Data Group, L. Montanet *et al.*, Phys. Rev. D **50**, 1173 (1994).
[24] J. Finjord, Phys. Lett. **76B**, 116 (1978); J. Finjord and M. K. Gaillard, Phys. Rev. D **22**, 778 (1980); H. Galic, D. Tadic, and J. Trampetic, Phys. Lett. **89B**, 249 (1980).
[25] G. Bunce, Nucl. Instrum. Methods **172**, 553 (1980).
[26] M. I. Adamovich *et al.*, Z. Phys. A **350**, 379 (1995).